Hindawi Publishing Corporation
Science and Technology of Nuclear Installations
Volume 2015, Article ID 460131, 15 pages
http://dx.doi.org/10.1155/2015/460131

Research Article

Alpha Stable Distribution Based Morphological Filter for Bearing and Gear Fault Diagnosis in Nuclear Power Plant

Xinghui Zhang,[1] Jianshe Kang,[1] Lei Xiao,[2] and Jianmin Zhao[1]

[1]*Mechanical Engineering College, Shijiazhuang 050003, China*
[2]*The State Key Lab of Mechanical Transmission, Chongqing University, Chongqing 400030, China*

Correspondence should be addressed to Xinghui Zhang; dynamicbnt@163.com

Received 28 February 2015; Revised 2 April 2015; Accepted 2 April 2015

Academic Editor: Arkady Serikov

Gear and bearing play an important role as key components of rotating machinery power transmission systems in nuclear power plants. Their state conditions are very important for safety and normal operation of entire nuclear power plant. Vibration based condition monitoring is more complicated for the gear and bearing of planetary gearbox than those of fixed-axis gearbox. Many theoretical and engineering challenges in planetary gearbox fault diagnosis have not yet been resolved which are of great importance for nuclear power plants. A detailed vibration condition monitoring review of planetary gearbox used in nuclear power plants is conducted in this paper. A new fault diagnosis method of planetary gearbox gears is proposed. Bearing fault data, bearing simulation data, and gear fault data are used to test the new method. Signals preprocessed using dilation-erosion gradient filter and fast Fourier transform for fault information extraction. The length of structuring element (SE) of dilation-erosion gradient filter is optimized by alpha stable distribution. Method experimental verification confirmed that parameter alpha is superior compared to kurtosis since it can reflect the form of entire signal and it cannot be influenced by noise similar to impulse.

1. Introduction

Nuclear power has 60 years' history from first nuclear plant constructed in Russia. In order to reduce carbon dioxide emissions, nuclear power is developed fast when the world enters 21st century. In existing nuclear power plants, some of them need to extend the operational life for coming 40 to 60 or possibly 60 to 80 years. In addition, for some newly nuclear power plants, they are expected to operate safely. Within these activities, there has been a strong awareness of the potential risk of both nuclear criticality and release of radioactive materials from generating electricity with nuclear power. Prognostics and health management (PHM) emerged and became a hot research topic for many scholars and research institutions. The effective application of PHM technologies will greatly reduce the possibility of accidents of nuclear power plants.

The main contents of PHM technology are fault detection, diagnosis, and prediction. Şeker et al. [1] applied Elman neural network to the condition monitoring of nuclear power plant and rotating machinery. Lee et al. [2] studied the condition monitoring of check valves in nuclear power plants based on acoustic emission (AE) signals. Zio and Popescu [3] used Kohonen self-organizing maps to diagnose the faults of gland seal system of a pump used in primary heat transport system. Ayaz [4] presented an anomaly detection method for Borssele nuclear power plant based on neural networks. He also conducted a comparison study for other important components in power plant. Jiang et al. [5] proposed a reliability Markov model to decrease the false alarms induced by human factors in condition monitoring process. Hashemian [6] discussed eight key online monitoring application technologies for nuclear power industry. They were detecting sensing-line blockages, testing the response time of pressure transmitters, monitoring the calibration of pressure transmitters online, cross calibrating temperature sensors in situ, assessing equipment condition, performing predictive maintenance of reactor internals, monitoring fluid flow, and extending the life of neutron detectors. Bond et al. [7] reviewed the condition based maintenance framework

of nuclear power plants with operational life over 60 years. Liu and Sheng [8] analyzed the possible gearbox condition monitoring scheme in high temperature reactor helium gas turbine system.

A nuclear reactor mainly consists of seven key components: fuel, moderators, control rods, shielding, coolant, turbines, and generator. Planetary gearbox is a key component for power transmission in nuclear reactor. Compared to the fixed-axis gearbox, planetary gearboxes are used in applications requiring low backlash, compact size, high efficiency, resistance to shock, and a high torque to weight ratio. In February 1999, the faults were found during the operation process of two circulating pumps driven by planetary gearboxes at Dayawan nuclear plant in China. Large area tooth spall fault had been found in sun gear and planet gear. Local pitting fault had been found in ring gear. In addition, slight wear also had been found in other teeth. Maintaining a good condition of planetary gearbox is very important for safety operation of nuclear power plant. Besides this, planetary gearbox is also widely used in other mechanical systems such as helicopters, wind turbines, and vehicles. Therefore, many scholars consider planetary gearbox to be an important research object. Vibration analysis has been widely accepted as one of the main techniques for condition based maintenance in rotating machinery for many years [9] and as the technique that provides more information about the condition of the gearbox. However, use of vibrations analysis technique is not restricted to condition monitoring; it also can be used for diagnostic purposes.

Park et al. [10] conducted a systematic failure analysis of the defect planetary gear carrier of tracked vehicle transmission. Wang et al. [11] investigated the wear between planet gear and thrust washer. The reasons for the wear failure also were exploited. Khazaee et al. [12] presented a powerful planetary gearbox fault diagnosis method through fusing the classification results of vibration and acoustic signals by Dempster-Shafer theory. Zimroz and Bartkowiak [13] proposed a novel way for condition monitoring of planetary gearboxes based on multivariate statistics. Then, data of two planetary gearboxes used in complex mining machines (one in bad machine and the other in good machine) were analyzed to verify the proposed method. Bartkowiak and Zimroz [14] researched the dimension reduction problem from linear and nonlinear approaches for the condition monitoring of planetary gearbox. Molina Vicuña [15] studied the influence of planetary gearbox AE signal by operating conditions. They acquired the results that influence of load in the resulting AE is significant at lower rotational speeds. However, at higher rotational speeds, the influence of load is masked by the influence of rotational speed. Feng and Liang [16] developed an adaptive optimal kernel time-frequency analysis to reveal the constituent frequency components of nonstationary signals and their time-varying features. Torregrosa Koch and Molina Vicuña [17] investigated the planetary gear fault detection through dynamic and phenomenological simulation model. Real fault data from two test benches also were used to compare. Liu et al. [18] developed a hybrid dimension reduction method combining kernel feature selection and kernel Fisher discriminant analysis. Then, it was used in planetary gearbox fault diagnosis. Hong et al. [19] used Fourier series analysis to explain the distinct sideband patterns which contain rich diagnostic information. They presented a formulation which can used to develop robust feature extraction algorithms for early detection of planetary gearbox failures. Chen et al. [20] proposed an ensemble method to analyze the nonstationary vibration signal of planetary gearbox. They processed the signal using multiwavelet transform in which the adaptive multiwavelet basis function was used. Finally, normalized ensemble multiwavelet transform information entropy is computed to track the degradation of planetary gearbox. The effectiveness was verified using the real fault data of planetary gearbox of ship-based communication antennas. Similar to the fixed shaft gearbox vibration signals, the signals of planetary gearbox also have amplitude and frequency modulation effect. Therefore, Feng et al. [21] proposed a fault diagnosis method for wind turbine planetary gearbox via demodulation analysis based on ensemble empirical mode decomposition and energy separation. Afterwards, Feng et al. [22] developed a new amplitude and frequency demodulation analysis method based on local mean decomposition for planetary gearbox fault diagnosis.

Nonlinear filter is the method which can enhance the fault diagnosis through eliminating the fault unrelated noise. Morphological gradient filter, a typical nonlinear filter, was first used in image processing. Nikolaou and Antoniadis [23] used four basic morphological operators (dilation, erosion, opening, and closing) to construct the envelope of impulsive type periodic vibration signals. Their effectiveness was examined by two defective industrial bearings. Authors claimed that a value of 0.6~0.7 times the fault frequency was appropriate for the effective length of structural element (SE). Li et al. [24] used weighted multiscale morphological gradient filter to diagnose the bearing faults. This method was compared with traditional envelope analysis and a multiscale enveloping spectrogram algorithm combining continuous wavelet transform and envelope analysis. Shen et al. [25] proposed an adaptive varying scale morphological analysis method. Experimental analysis demonstrated that varying scale morphological operators has fast computation speed in comparison to multiscale morphological operators. To separate the mixed sources from a single channel signal, Dong et al. [26] proposed a repeated blind source separation method based on morphological filtering and singular value decomposition. Authors used morphological filter to remove noise which would affect the accuracy of the separation. Li and Xiao [27] proposed a new fault diagnosis method based on one-dimensional adaptive rank-order morphological filter. In [28], the SEs were constructed with two parabolas while four parameters were optimized using genetic algorithm. The proposed method was validated using vibration signals collected from pump and motor engine. Tan et al. [29] developed an optimal multiscale morphological filter. The average of the closing and opening operator was used to construct the morphological filter. Further, the multiscale morphological filter's SEs were optimized and selected by particle swarm optimization algorithm. Raj and Murali [30]

used morphological operators and fuzzy inference to classify the bearing fault. Chen et al. [31] proposed a signal based triangular SE for mathematical morphological operation and applied this to rolling element bearing fault diagnosis. The SE was constructed according to the statistics of the magnitude of vibration signal. As we know, the effectiveness of morphological technique not only relies on operation but also relies on the SE. For engineering application, the computation time of morphological filtering is very short and can be used for online fault diagnosis.

To optimize the length of SE signal to noise ratio (SNR) and kurtosis can be used. In another view, specific SE can be constructed for fault diagnosis. Recently, a new statistical method called stable distribution has been used for bearing fault diagnosis [32]. In order to determine the optimal frequency band, authors used alpha parameter of stable distribution for envelope analysis in order to determine the optimal frequency band. In this paper, we constructed a new morphological gradient filter with optimized length of SE by alpha parameter and verified its effectiveness for the bearing and planetary gears fault diagnosis. This is also the main contribution of this paper. Dilation-erosion operator is used as the filter because it is superior to other morphological operators. A detailed bearing fault test rig data, bearing simulation data, and planetary gearbox gears fault study was conducted, in process of method effectiveness verification. In case studies, alpha parameter is compared to the kurtosis.

To explain the proposed method, this paper is organized as follows. Section 2 gives a brief review of the stable distribution and morphological gradient filter. Section 3 presents development of a new fault diagnosis framework based on stable distribution and morphological gradient filter. Section 4 demonstrates the effectiveness of proposed method using one simulation faulty bearing data and planetary gearbox gears faulty data with sun gear, planet gear, and ring gear fault tested separately. Finally, Section 5 gives a conclusion of the work.

2. Basic Review of Stable Distribution and Morphological Gradient Filter

2.1. Stable Distribution. "In probability theory, a random variable is said to be stable (or to have a stable distribution) if it has the property that a linear combination of two independent copies of the variable has the same distributions, up to location and scale parameters". The stable distribution family is also sometimes referred to as the "Lévy alpha stable distribution" [33]. It allows skewness and heavy tails and has many mathematical properties and also does not have closed form for probability density and cumulative distribution function. With computers power increasing it is simple to estimate the parameters and apply the stable distribution to various engineering problem.

In this paper, two generally major stable distribution parameters are used. One is called 0-parameterization and the other is called 1-parameterization. These two parameterizations can be defined as follows [34].

Definition 1. A random variable X is $\mathbf{S}(\alpha, \beta, \gamma, \delta; 0)$ if

$$X \overset{d}{=} \begin{cases} \gamma\left(Z - \beta\tan\dfrac{\pi\alpha}{2}\right) + \delta, & \alpha \neq 1, \\ \gamma Z + \delta, & \alpha = 1, \end{cases} \tag{1}$$

where $Z = Z(\alpha, \beta)$ is a random variable with characteristic function

$$E\exp(iuZ) = \begin{cases} \exp\left(-|u|^{\alpha}\left[1 - i\beta\tan\dfrac{\pi\alpha}{2}(\operatorname{sign} u)\right]\right), & \alpha \neq 1, \\ \exp\left(-|u|\left[1 + i\beta\dfrac{2}{\pi}(\operatorname{sign} u)\log|u|\right]\right), & \alpha = 1, \end{cases} \tag{2}$$

and X has characteristic function

$$E\exp(iuX) = \begin{cases} \exp\left(-\gamma^{\alpha}|u|^{\alpha}\left[1 + i\beta\left(\tan\dfrac{\pi\alpha}{2}\right)\right.\right. \\ \qquad \left.\left. \cdot(\operatorname{sign} u)\left(|\gamma u|^{1-\alpha} - 1\right)\right] + i\delta u\right), \\ \qquad\qquad \alpha \neq 1, \\ \exp\left(-\gamma|u|\left[1 + i\beta\dfrac{2}{\pi}(\operatorname{sign} u)\log(\gamma|u|)\right] + i\delta u\right), \\ \qquad\qquad \alpha = 1. \end{cases} \tag{3}$$

Definition 2. A random variable X is $\mathbf{S}(\alpha, \beta, \gamma, \delta; 1)$ if

$$X \overset{d}{=} \begin{cases} \gamma Z + \delta, & \alpha \neq 1, \\ \gamma Z + \left(\delta + \beta\dfrac{2}{\pi}\gamma\log\gamma\right), & \alpha = 1; \end{cases} \tag{4}$$

X has a characteristic function

$$E\exp(iuX) = \begin{cases} \exp\left(-\gamma^{\alpha}|u|^{\alpha}\left[1 - i\beta\left(\tan\dfrac{\pi\alpha}{2}\right)(\operatorname{sign} u)\right] + i\delta u\right), \\ \qquad\qquad \alpha \neq 1, \\ \exp\left(-\gamma|u|\left[1 + i\beta\dfrac{2}{\pi}(\operatorname{sign} u)\log(|u|)\right] + i\delta u\right), \\ \qquad\qquad \alpha = 1. \end{cases} \tag{5}$$

From these two definitions, we can see that there are four distribution parameters. α is the tail index, or index of stability, with values in range $0 \leq \alpha \leq 2$, β is skewness parameter with values in range $-1 \leq \beta \leq 1$, γ is scale parameter and must be positive, and δ is a location parameter, an arbitrary real number.

These parameters can be estimated through seven methods: maximum likelihood method, quantile method, empirical characteristic function, fractional moment method, log absolute moment method, modified quantile method, and U statistic method. Figures 1–3 are showing probability density function (PDF) variations when one parameter varies and the other three parameters are fixed. Variation of parameter β has no obvious effect of the PDF form. Therefore, only parameters α, γ, and δ are illustrated.

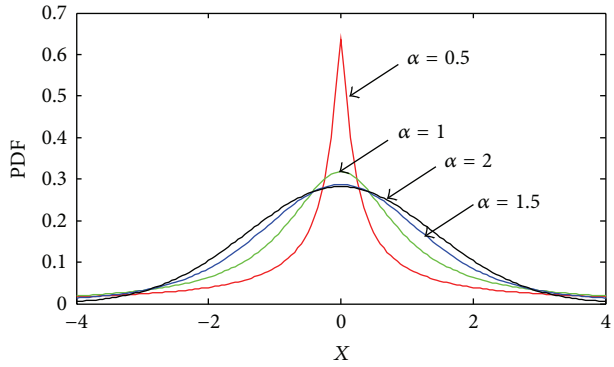

Figure 1: PDF of stable distribution with different α values ($\beta = 0, \gamma = 1, \delta = 0$).

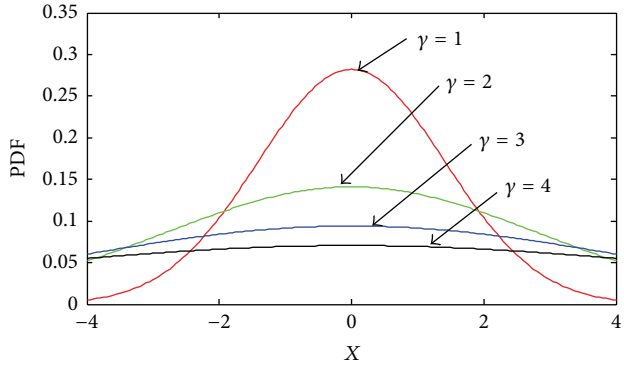

Figure 2: PDF of stable distribution with different γ values ($\alpha = 2, \beta = 0, \delta = 0$).

2.2. Morphological Gradient Filter. Suppose $s(n)$ is the one dimensional vibration signal and $v(n)$ is the SE. The four basic morphological operators can be described as follows:

Opening:

$$(s \circ v)(n) = (s\Theta v \oplus v)(n), \quad n = 0, 1, 2, \ldots, N-1. \tag{6}$$

Closing:

$$(s \bullet v)(n) = (s \oplus v\Theta v)(n), \quad n = 0, 1, 2, \ldots, N-1. \tag{7}$$

Dilation:

$$(s \oplus v)(n) = \max[s(n-m) + v(m)], \quad m = 0, 1, 2, \ldots, M-1, \quad n = 0, 1, 2, \ldots, N-1. \tag{8}$$

Erosion:

$$(s\Theta v)(n) = \min[s(n+m) - v(m)], \quad m = 0, 1, 2, \ldots, M-1, \quad n = 0, 1, 2, \ldots, N-1. \tag{9}$$

Notations $\Theta, \oplus, \circ$, and $\bullet$ denote operations of erosion, dilation, opening, and closing, respectively. The dilation can broaden the width of positive peaks and reduce the width of negative peaks of vibration signal. However, the erosion will give inverse effect. The opening and closing operation can remove positive and negative impulses while preserving other pieces of information. These four fundamental operators can be combined and form other new morphological operators such as opening-closing operator and dilation-erosion operator.

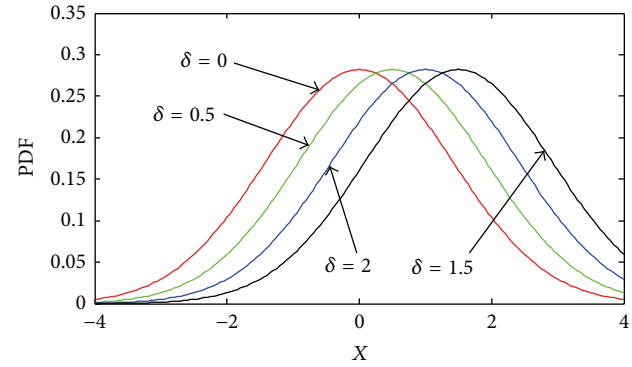

Figure 3: PDF of stable distribution with different δ values ($\alpha = 2, \beta = 0, \gamma = 1$).

The filtering effect of morphological technique relies not only on the morphological operator, but also on the structure of structuring element (SE). The SE contains flat SE and nonflat SE. In this paper, a kind of flat SE-line SE is used. The only parameter of this SE is the length. Raj and Murali [30] used kurtosis to optimize the length of SE. In this paper, parameter α of stable distribution will be used to optimize the length of SE and compared to the kurtosis based optimization.

3. Fault Diagnosis Framework Based on Stable Model and Morphological Gradient Filter

The detailed diagnosis process is explained in this Section. Suppose the vibration signal of mechanical components follows stable distribution. Then, parameters can be estimated using relevant methods. In order to explain the function of stable model in mechanical fault diagnosis, bearing fault data from Case Western Reserve University are used [35]. The motor shaft was supported by 6205-2RSJEM bearings. The bearing faults were implanted using electrodischarge machining with fault sizes: 0.007 inches, 0.014 inches, and 0.021 inches. The accelerometers were used to collect vibration signals at 12 k Hz and the outer race faults were implanted at 3 o'clock, 6 o'clock, and 12 o'clock positions, respectively.

Here, for framework description data sets of normal, inner race fault, ball fault, and outer race fault at six o'clock position under 1797 rpm and 0 HP load are used first. To estimate the parameters of stable distribution 0-parameterization and empirical characteristic function are used. Different fault mode has different PDF shape in comparison of PDF versus the fault signal, shown in Figure 4.

Further, normal bearing data and inner race fault data of three different fault severities under condition 1,797 rpm and 0 HP load are used to analyze different severity. The results are shown in Figure 5.

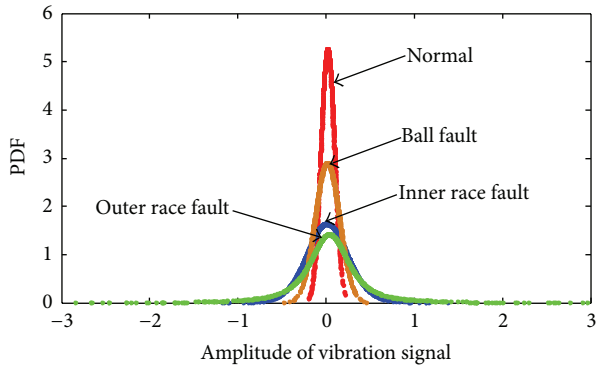

Figure 4: PDF of bearing fault vibration signal.

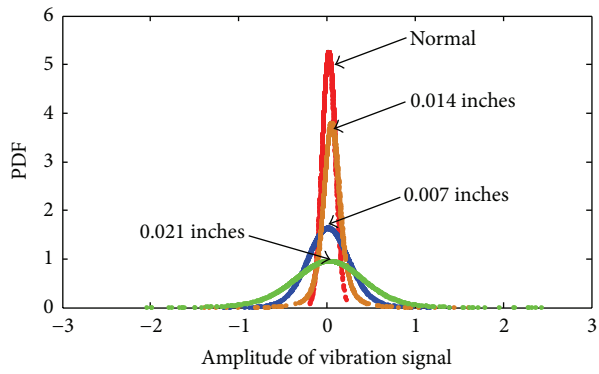

Figure 5: PDF of bearing fault vibration signal.

From Figures 4 and 5, we can see that distribution shapes are very similar to stable distribution shown in Figure 1. Therefore, the parameter α is a very important indicator to reflect the faults for bearing fault diagnosis and at the same time rotating machinery fault diagnostics. Usually, α equals 2 for undamaged bearing condition state and its value will decrease with the fault propagation. In other words, parameter α has strong relation to the impulse signal becoming dominant with fault progression. This feature can be used to reflect the strength of impulse signal and to evaluate the morphological gradient filter length of SE.

After the framework description of stable distribution model in rotating machinery fault diagnosis, morphological gradient filter is discussed. Data of inner race bearing fault under condition 1,797 rpm and 0 HP load with 0.007 inches fault size is used. In order to reduce the computational process maximum length of SE cannot exceed the fault period. Only certain proportion of fault period is used as the length of SE: 0.1, 0.2, 0.3, 0.4, 0.5, 0.6, 0.7, 0.8, and 0.9 times fault period which makes totally nine scales of SE. In order to compare the effectiveness of different morphological operator, only 0.1 times fault period is used as the length of SE. The results of different morphological operator for 0.1 times fault period and frequency spectrum are shown in Figures 6–11.

Bearing fault frequencies are defined as ball pass frequency inner race (BPFI), ball pass frequency outer race (BPFO), ball spin frequency (BSF), and fundamental train frequency (FTF). The characteristic fault frequencies are calculated through the geometric parameters of 6205 bearings: BPFO (107.36 Hz), BPFI (162.18 Hz), BSF (141.17 Hz), and FTF (11.93 Hz).

Observing the frequency spectrums from Figures 6–11 it is evident that dilation-erosion gradient filter has the very good performance for enhancing the impulse signal. The frequency spectrum of signal after dilation-erosion filter has the highest amplitude of BPFI frequency compared to those acquired by other operators. This is the main reason why dilation-erosion operator is selected.

The framework of rotating machinery fault diagnosis method based on stable distribution and morphological gradient filter is shown in Figure 12 and detailed process can be explained as follows:

(1) First, the vibration signal is acquired. If tachometer signal is acquired simultaneously, the vibration signal should be resampled according to the tachometer signal producing stationary signal representing synchronous-angular sampling. We call it time synchronous signal.

(2) Second, the time synchronous signal is processed by morphological gradient filter with different length of SE.

(3) Third, the filtered signal with minimum α value is selected as the final signal for frequency analysis.

(4) Finally, the fault frequencies can be tracked using frequency analysis.

4. Proposed Method Verification

4.1. Proposed Method Verification Using Bearing Faults Simulation Data. The simulated bearing fault signal with single resonant frequency similar to signal in [36] is given as follows:

$$y(t) = y_0 e^{-\xi \times 2\pi f_n \times t - \tau} \sin\left(2\pi f_n \times \sqrt{1-\xi^2} \times t - \tau\right), \quad (10)$$

where ξ is equal to 0.1, f_n is the resonant frequency equal to 2,600 Hz, and τ is used to simulate the randomness caused by slippage which is subject to a discrete uniform distribution. y_0 (equal to 1.5) is the amplitude of the simulated bearing impulse signal. Suppose the sampling frequency is 12,000 Hz. Then, the bearing fault signal is simulated according to the fault frequency (equal to 100 Hz). A total of 24,000 samplings were used for each simulated signal. Finally, a random signal with a mean of zero and the standard deviation of 0.6 were added to (10).

According to the framework in Section 3, this bearing fault signal can be processed using dilation-erosion gradient filter with different length of SE. In order to explain the proposed method in detail, three lengths of fault signal are used. They are 16,384, 131,072, and 240,000. Because the fault frequency is equal to 100 Hz and the sampling frequency is 12,000 Hz that gives the fault period of 120 samples. As mentioned in Section 3, nine lengths of SE are used. They are 0.1 × 120, 0.2 × 120, 0.3 × 120, 0.4 × 120, 0.5 × 120, 0.6 × 120, 0.7 × 120, 0.8 × 120, and 0.9 × 120. Those nine lengths of SEs and

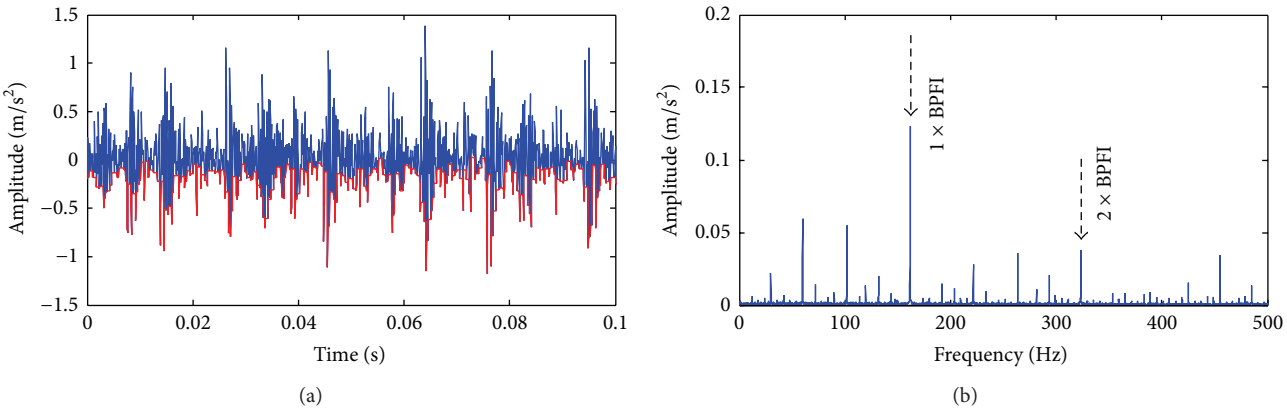

Figure 6: (a) Results of morphological operation opening; (b) frequency spectrum of (a).

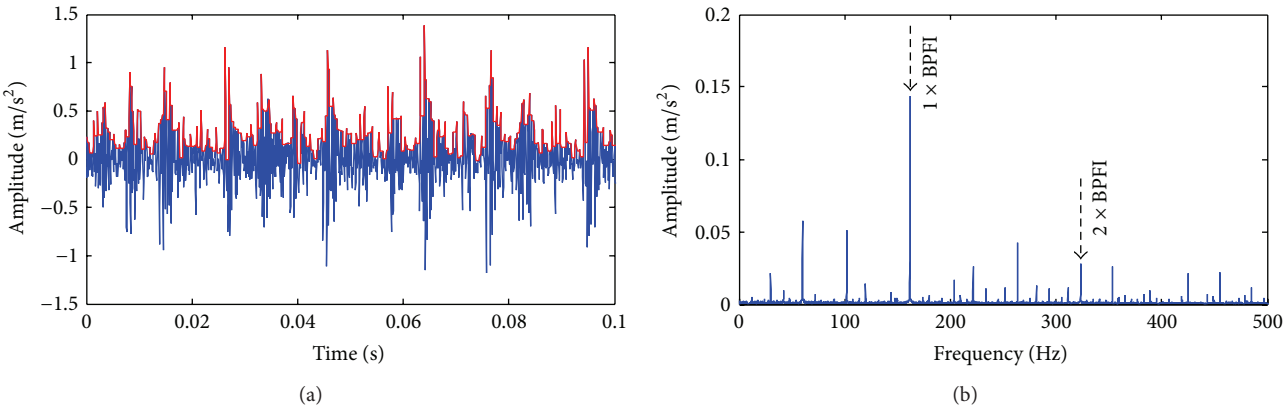

Figure 7: (a) Results of morphological operation closing; (b) frequency spectrum of (a).

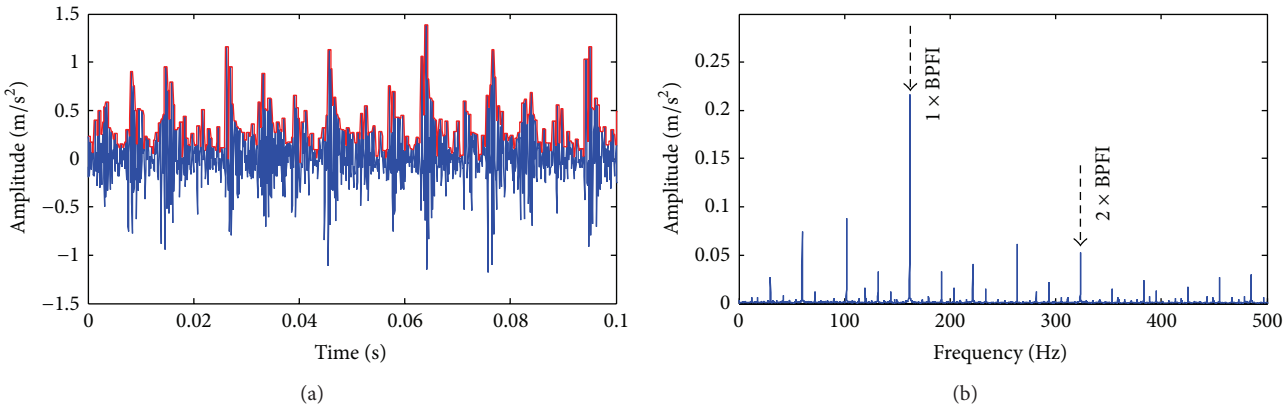

Figure 8: (a) Results of morphological operation dilation; (b) frequency spectrum of (a).

both α and kurtosis are used to evaluate the effect in order to find optimal scale (length of SE). The results are shown in Figures 13–18.

Kurtosis and α value of different length of SE for 16,384 samples are shown in Figures 13(a) and 13(b). The ninth length of SE is the optimal scale determined by kurtosis value and the first SE is the optimal scale (length of SE) determined by α value. From frequency spectrum shown in Figure 14(a), filtered signal by first length of SE, it is possible to locate the fault frequency and its harmonics, while for ninth length of SE it is impossible, Figure 14(b).

Similarly, kurtosis and α value for 131,072 samples and different length of SE are shown in Figures 15(a) and 15(b). The ninth length of SE is the optimal scale determined by

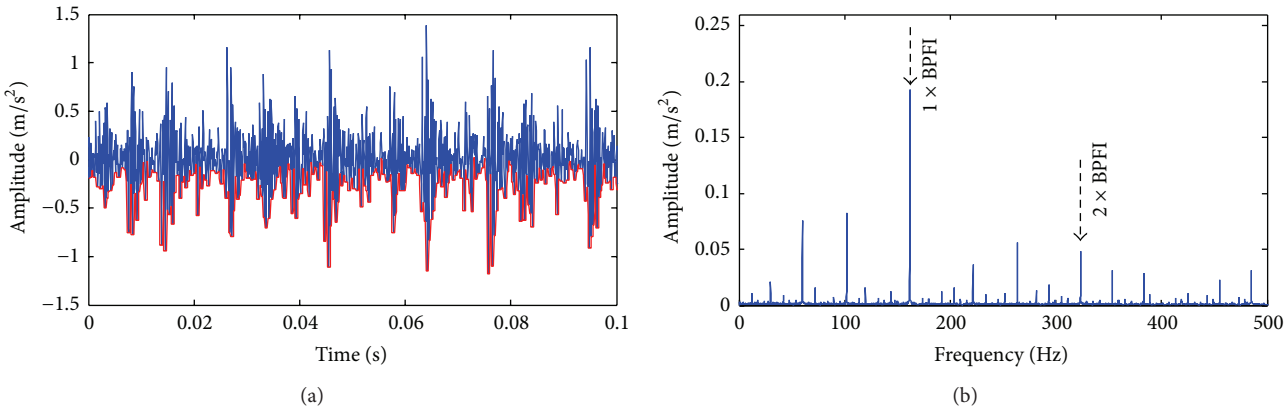

Figure 9: (a) Results of morphological operation erosion; (b) frequency spectrum of (a).

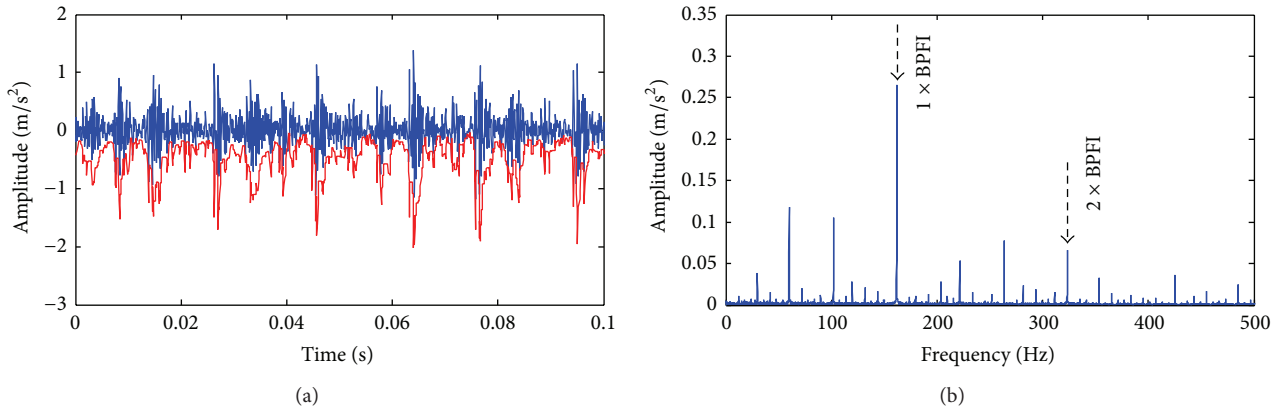

Figure 10: (a) Results of morphological operation open-close gradient; (b) frequency spectrum of (a).

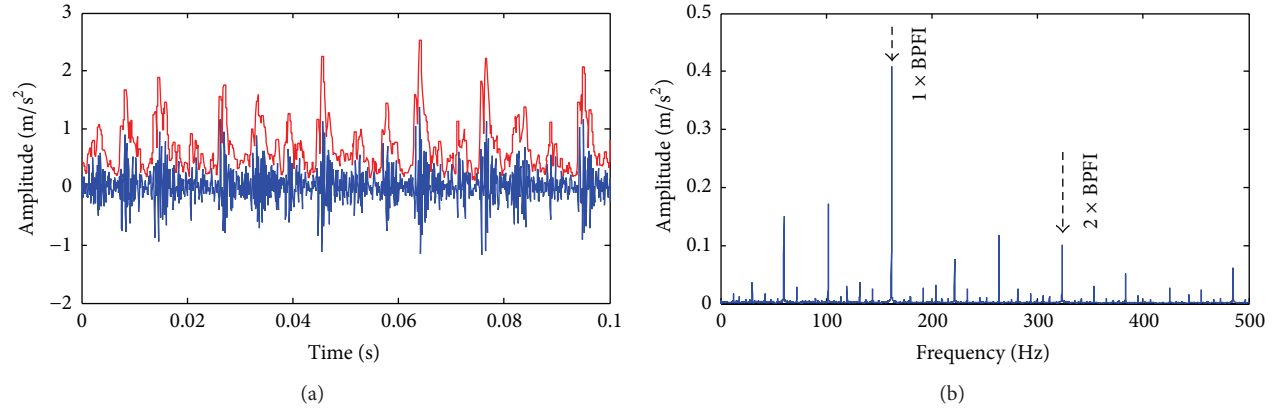

Figure 11: (a) Results of morphological operation dilation-erosion gradient; (b) frequency spectrum of (a).

kurtosis value in this case and second length of SE is the optimal scale determined by α value. Using both filtered signals, second and ninth length of SE, it is possible to locate fault frequency and its harmonics, shown in Figure 16. What is more, the frequency spectrum acquired by ninth SE has strong noise at frequency in range [0 100] Hz.

Both frequency spectrums of filtered signals by two methods have fault frequency and harmonics for 240,000 samples shown in Figure 17. However, result acquired by first length of SE is more obvious in comparison to the result acquired by second length of SE shown in Figures 17 and 18.

Through these three different sample lengths analysis, we can conclude that the optimal length of SE determined by α value is more stable than kurtosis. In the following planetary gearbox gear fault case study method verification, α value of stable distribution is used to determine the optimal SE length.

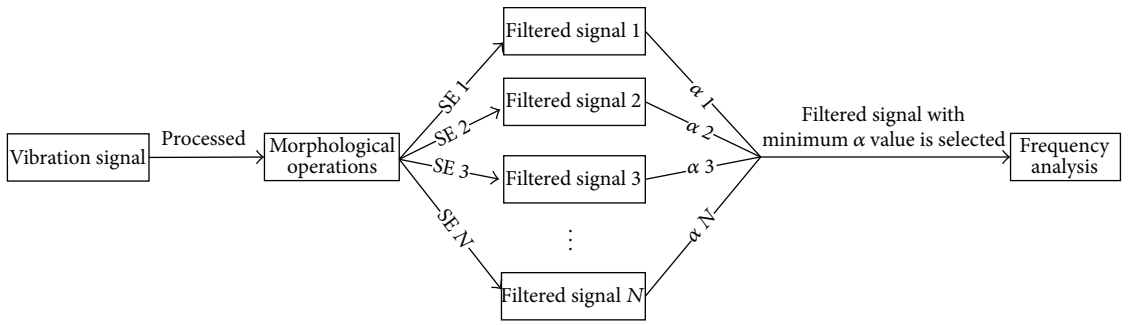

Figure 12: Framework of proposed diagnosis method based on stable distribution and morphological gradient filter.

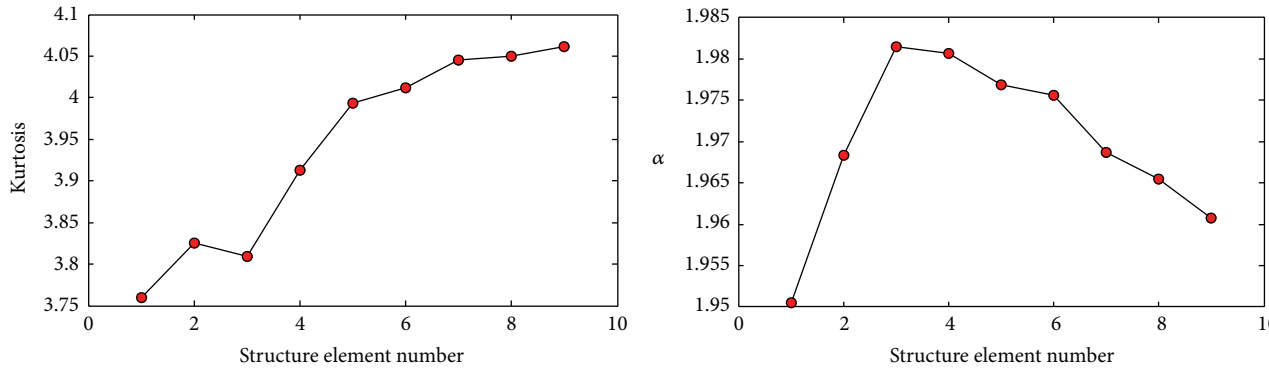

Figure 13: (a) Kurtosis value versus length of SE for 16,384 samples; (b) α value versus length of SE for 16,384 samples.

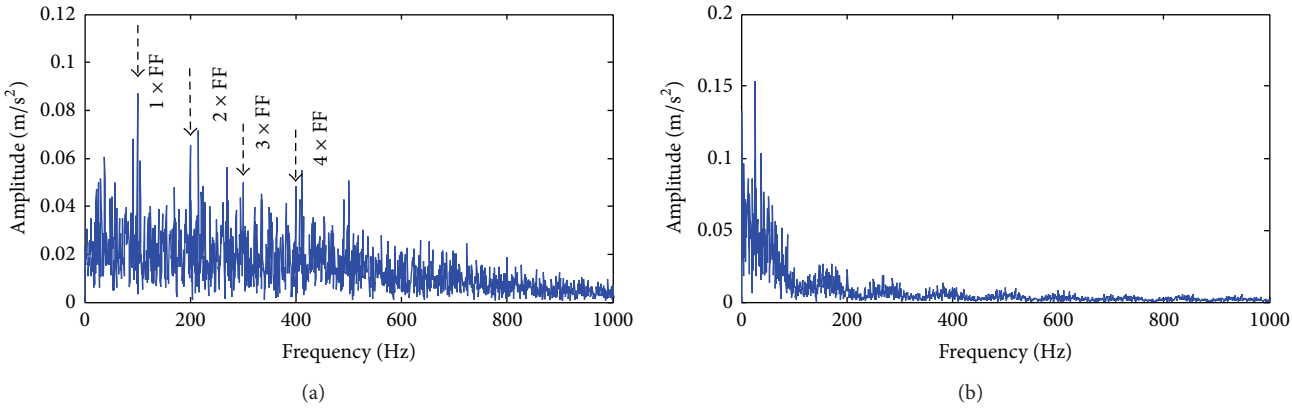

Figure 14: (a) Frequency spectrum of filtered signal by first length of SE; (b) frequency spectrum of filtered signal by ninth length of SE.

Beside this, another small case can be used for further verification superiority of α value. Gaussian signal with standard deviation 0.6 shown in Figure 19 is used and Gaussian signal which added an impulse noise is shown in Figure 20. In reality, its kurtosis value will be near to 3 and α value near to 2. PDF of Gaussian signal with impulsive noise is shown in Figure 21. Comparing the kurtosis and α value of Gaussian signal with and without impulsive noise, it is evident that the impulsive noise has limited influence on α value but great influence on kurtosis value. Therefore, α is more stable than kurtosis for fault estimation and PDF shape has no great variation with presence of the impulsive noise. Only an abnormal point circle (marked red) can be found, shown in Figure 21.

4.2. Proposed Method Verification for Gears Fault Diagnosis of Planetary Gearbox. Figure 22 illustrates an experimental one-stage planetary gearbox test rig. As shown in Figure 23, it comprises one sun gear, three planet gears, and one ring gear. Single stage planetary gearbox gear parameters are listed in Table 1.

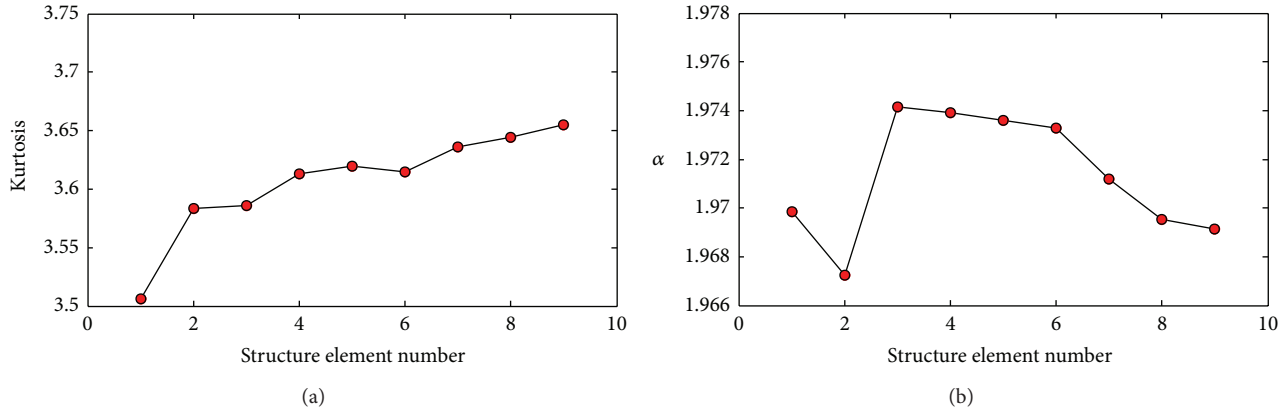

Figure 15: (a) Kurtosis value versus length of SE for 131,072 samples; (b) α value versus length of SE for 131,072 samples.

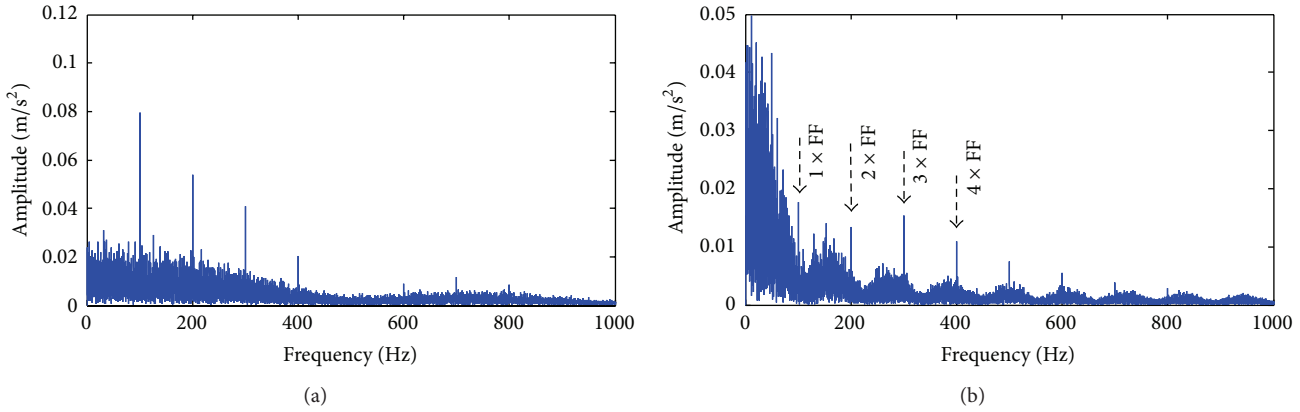

Figure 16: (a) Frequency spectrum of filtered signal by second length of SE; (b) frequency spectrum of filtered signal by ninth length of SE.

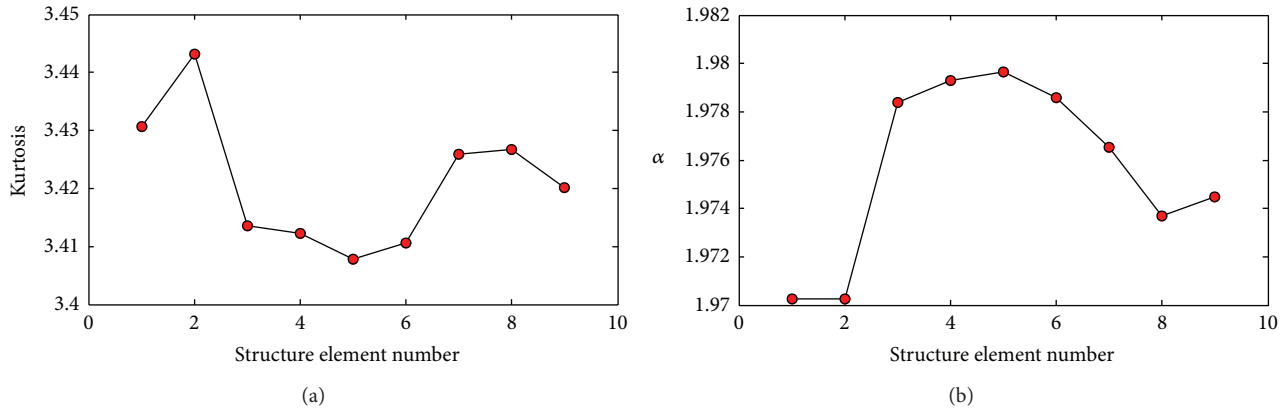

Figure 17: (a) Kurtosis value versus length of SE for 240,000 samples; (b) α value versus length of SE for 240,000 samples.

Table 1: Gear parameters of single stage planetary gearbox.

Gear	Sun	Planet	Ring	Planet number
Teeth number	13	64	146	3

It includes a single stage planetary gearbox, a 4 kW three-phase asynchronous motor for driving the gearbox, and a magnetic powder brake for loading. The motor speed can be adjusted for different value. The load can be adjusted by a brake controller through current of magnetic powder brake connected to the output shaft (carrier). The NI

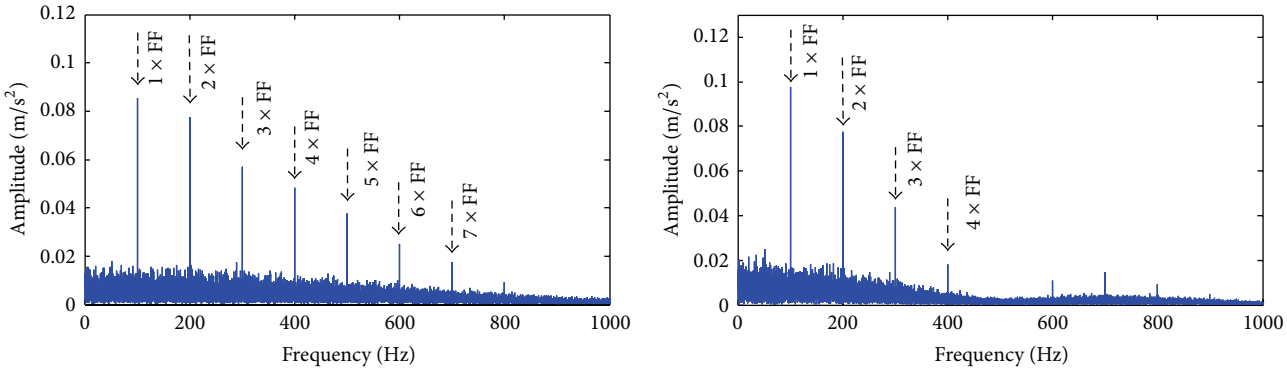

Figure 18: (a) Frequency spectrum of filtered signal by first length of SE; (b) frequency spectrum of filtered signal by second length SE.

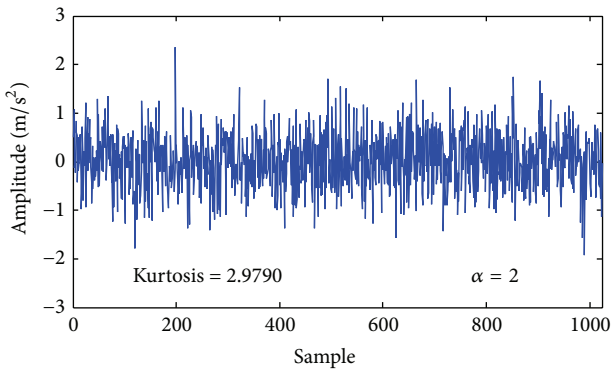

Figure 19: Gaussian signal with standard deviation 0.6.

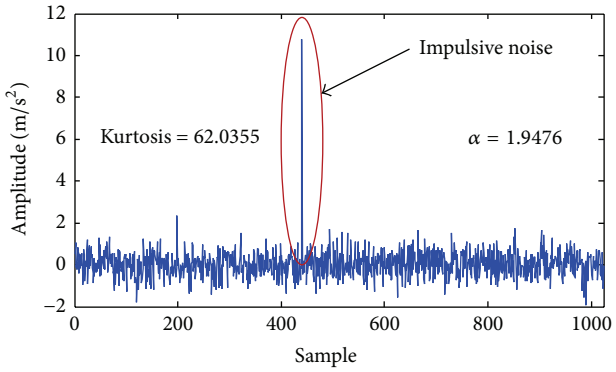

Figure 20: Gaussian signal added impulsive noise.

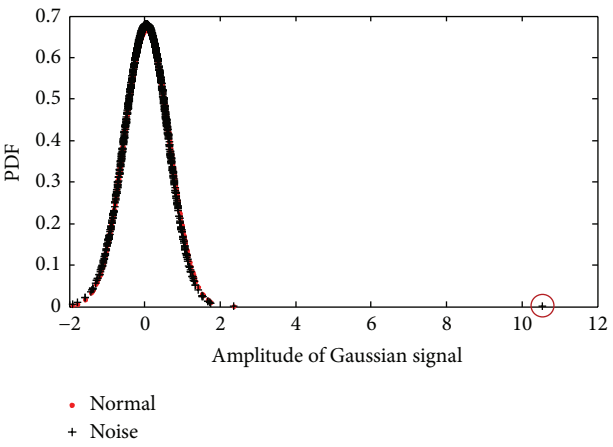

Figure 21: PDF of Gaussian signal added impulsive noise.

data acquisition system consists of four IEPE accelerometers (Dytran 3056B4), PXI-1031 mainframe, PXI-4472B data acquisition cards, and LabVIEW software. In addition, a tachometer and torque sensor is installed in the input shaft for acquiring the speed and load information.

In this study, only data for input shaft speed of 1,200 rpm with a load of 405 Nm was applied to the output shaft connecting planet carrier. The sampling frequency was 20 kHz for duration of 12 seconds. Wear gears faults of planetary gearbox were implanted in one tooth of ring gear, planet gear, and sun gear, respectively, in order to verify the proposed method. An accelerometer was mounted on the top of the gearbox casing (as shown in Figure 22), and the vibration signals were collected from accelerometer at position S3. Figure 24 illustrates implanted gear wear faults.

Tooth wear faults belong to localized fault and their fault frequencies can be calculated through following equations [37]:

Planet gear fault frequency:

$$f_{\text{planet1}} = \frac{f_{\text{mesh}}}{Z_{\text{planet}}},$$
$$f_{\text{planet2}} = 2\frac{f_{\text{mesh}}}{Z_{\text{planet}}}. \tag{11}$$

Sun gear fault frequency:

$$f_{\text{sun}} = \frac{f_{\text{mesh}}}{Z_{\text{sun}}} N_{\text{planet}}. \tag{12}$$

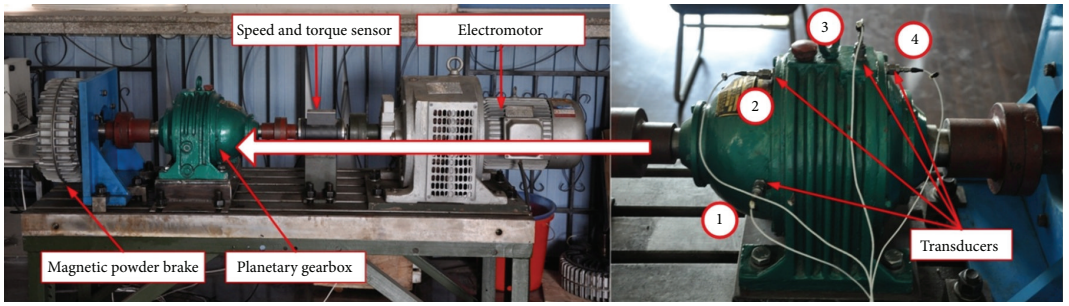

Figure 22: Planetary gearbox fault test rig.

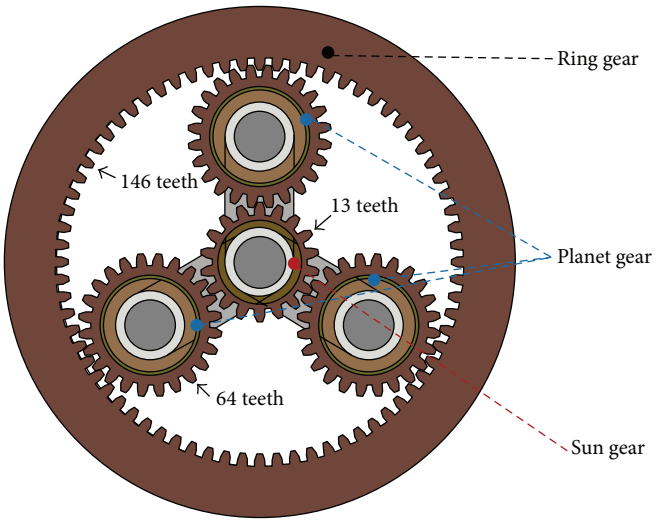

Figure 23: Schematic map of planetary gearbox structure.

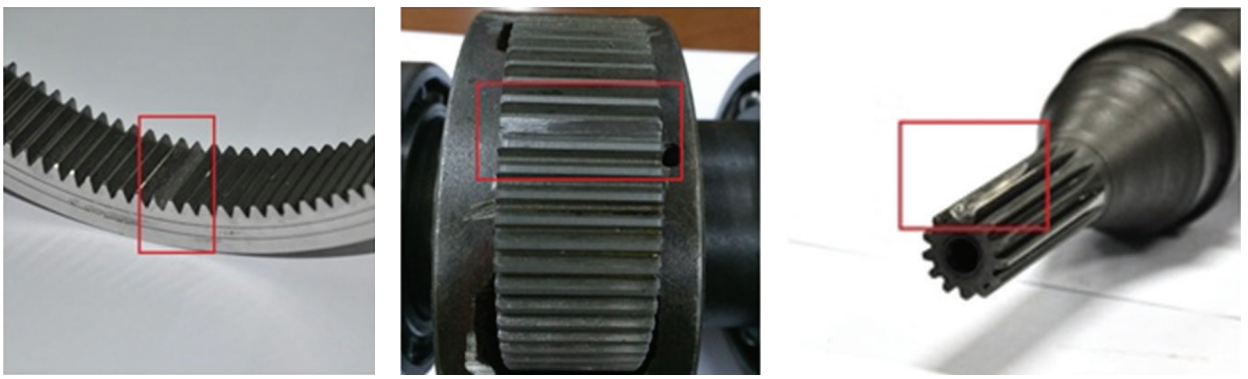

(a) (b) (c)

Figure 24: Implanted wear fault: (a) ring gear, (b) planet gear, and (c) sun gear.

Ring gear fault frequency:

$$f_{\text{ring}} = \frac{f_{\text{mesh}}}{Z_{\text{ring}}} N_{\text{planet}}. \tag{13}$$

In these equations, f_{mesh} denotes the mesh frequency, f_{planet} denotes the planet gear fault frequency, f_{sun} denotes the sun gear fault frequency, and f_{ring} denotes the ring gear fault frequency. Z_{sun} denotes the tooth number of sun gear, Z_{ring} denotes the tooth number of ring gear, and N_{planet} denotes the planet gear number.

The mesh frequency can be calculated by

$$f_{\text{mesh}} = f_{\text{carrier}} \times Z_{\text{ring}}. \tag{14}$$

Table 2: Characteristic frequencies (Hz).

Meshing frequency	Rotating frequency		Fault frequencies			
	Sun	Carrier	Planet		Sun	Ring
239.8183	20.0889	1.6425	3.7472	7.4944	55.3427	4.9278

Table 3: Characteristic frequencies (Hz).

Meshing frequency	Rotating frequency		Fault frequencies			
	Sun	Carrier	Planet		Sun	Ring
238.8748	20.0111	1.6361	3.7324	7.4648	55.1249	4.9083

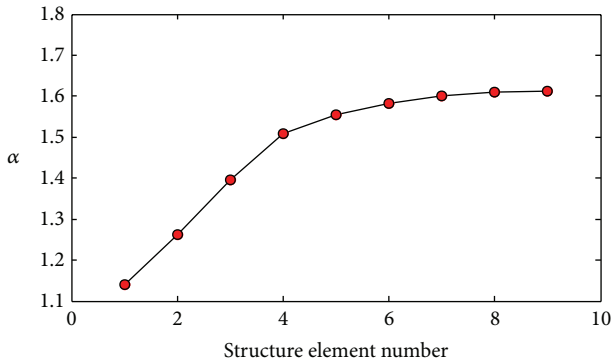

Figure 25: α value versus the different SE length.

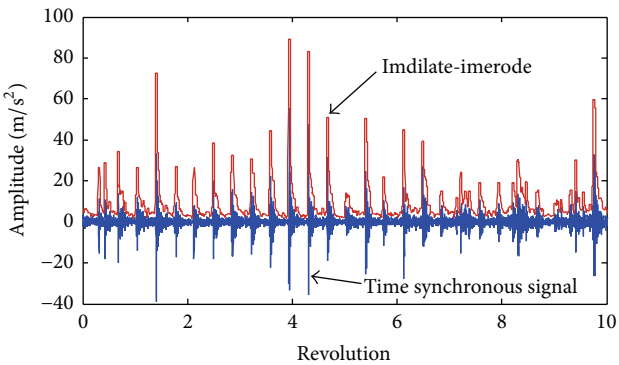

Figure 26: Result of morphological dilation-erosion gradient.

4.2.1. Sun Gear Fault Case. During experiment, the mean rotating frequency of the input shaft connecting sun gear of planetary gearbox was 20.0889 Hz while a load of 405 Nm was applied to the output shaft connecting planet carrier. An accelerometer was mounted on the top of the gearbox casing (as shown in Figure 23), and the vibration signals were collected from accelerometer at position S3. According to the planetary gearbox configuration and its running speed, the characteristic frequencies are calculated and listed in Table 2.

Dilation-erosion operator is used to filter the signal. α value versus the different SE length is shown in Figure 25. It shows the first length is optimal. Figure 26 is the time envelope by dilation-erosion operator with first SE length.

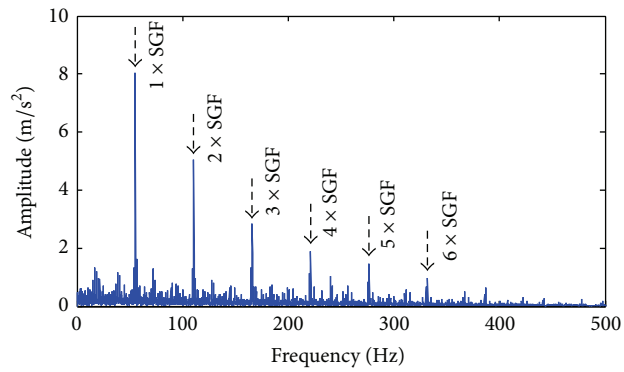

Figure 27: Frequency spectrum of filtered signal.

Frequency spectrum of resulted signal shows strong sun gear fault frequency and harmonics and demonstrates the effectiveness of proposed method shown in Figure 27.

4.2.2. Planet Gear Fault Case. During experiment, the mean rotating frequency of the input shaft connecting sun gear of planetary gearbox was 20.0111 Hz while a load of 405 Nm was applied to the output shaft connecting planet carrier. An accelerometer was mounted on the top of the gearbox casing and the vibration signals were collected from accelerometer at position S3. According to the planetary gearbox configuration and its running speed, the characteristic frequencies are calculated and listed in Table 3.

Similarly, the optimal length of SE is determined by α value shown in Figure 28. The planet fault frequency is very low. In other words, the samples in one period are very big. Therefore, 0.01, 0.02, 0.03, 0.04, 0.05, 0.06, 0.07, 0.08, and 0.09 times fault period are used as the length of SE. The first length is optimal. The corresponding frequency spectrum of filtered signal by dilation-erosion gradient filter is shown in Figure 29. It can be seen that there are the planet fault frequency f_{planet2} (second order of f_{planet1}) and second-order planet fault frequency (fourth order of f_{planet1}). In addition, planet fault frequency plus carrier frequency is also found and also signatures of planet gear fault are more obvious.

4.2.3. Ring Gear Fault Case. In this case, ring gear fault data under approximate 1,200 rpm and 405 Nm load is used for processing. Similarly, it is resampled according

Table 4: Characteristic frequencies (Hz).

Meshing frequency	Rotating frequency		Fault frequencies			
	Sun	Carrier	Planet		Sun	Ring
267.2586	22.3889	1.8305	4.1759	8.3518	61.6751	5.4916

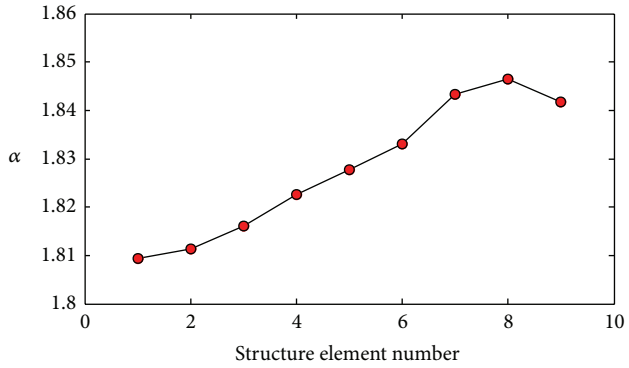

Figure 28: α value versus the different length of SE.

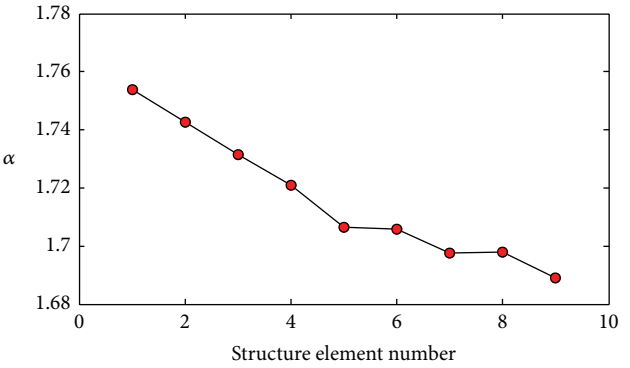

Figure 30: α value versus the different SE length.

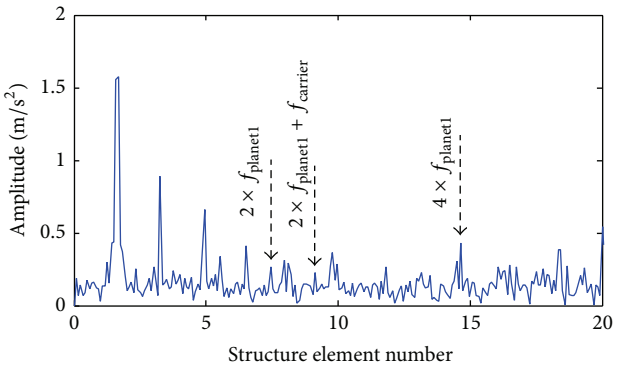

Figure 29: Frequency spectrum of filtered signal.

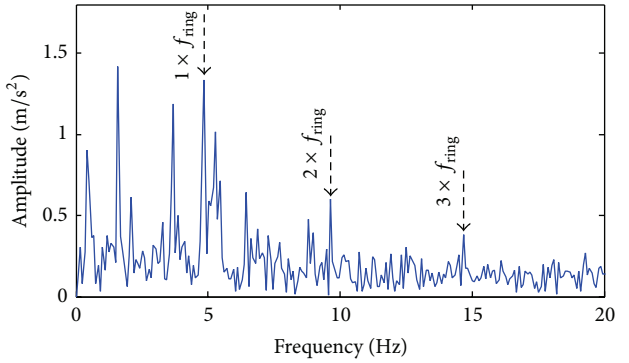

Figure 31: Frequency spectrum of filtered signal.

to the tachometer signal. The mean rotating frequency is 22.3889 Hz. So, new planetary gearbox fault frequencies can be shown in Table 3.

During experiment, the mean rotating frequency of the input shaft connecting sun gear of planetary gearbox was 22.3889 Hz while a load of 405 Nm was applied to the output shaft connecting planet carrier. An accelerometer was mounted on the top of the gearbox casing and the vibration signals were collected from accelerometer at position S3. According to the planetary gearbox configuration and its running speed, the characteristic frequencies are calculated and listed in Table 4.

Optimal length of SE is acquired through α value and is shown in Figure 30. The corresponding frequency spectrum is shown in Figure 31 and obvious ring gear fault frequency and its harmonics can be observed. This case also demonstrates the effectiveness of proposed method.

In order to verify the stable distribution on fault diagnosis continuously, the PDFs of normal, sun gear fault, planet gear fault, and ring gear fault are shown in Figure 32. This demonstrates the effectiveness of parameter α for different planetary gears fault.

5. Conclusions

In this paper, a new planetary gearbox fault diagnosis method based on stable distribution and morphological gradient filter is proposed. Using morphological gradient filter we proved that parameter α- of stable distribution is superior to kurtosis in process of selection of the optimal length of SE. Comparing six different morphological operators, dilation-erosion operators are selected to extract the envelope of signal. The framework of proposed method is explained in detail. Finally, a simulation case and an experimental planetary gearbox fault case are used to demonstrate the effectiveness of proposed method. In future, the degradation of planetary gearbox will be investigated using the same method.

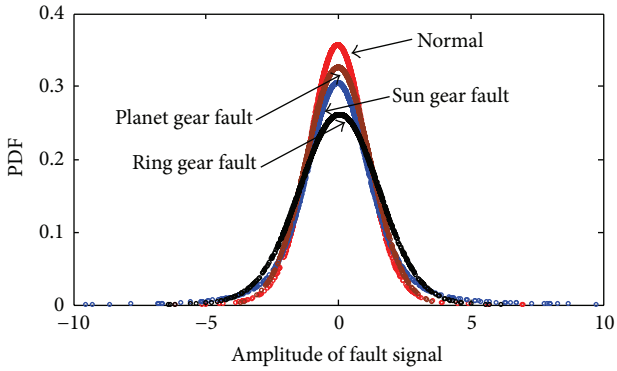

FIGURE 32: PDF of planetary gearbox fault vibration signal.

Conflict of Interests

The authors declare that there is no conflict of interests regarding the publication of this paper.

Acknowledgments

The parameters of stable distribution are estimated by program developed by Robust Analysis, Inc. This project was partially supported by Natural Science Foundation of Hebei Province Reference (E2015506012) and China Scholarship Council.

References

[1] S. Şeker, E. Ayaz, and E. Türkcan, "Elman's recurrent neural network applications to condition monitoring in nuclear power plant and rotating machinery," *Engineering Applications of Artificial Intelligence*, vol. 16, no. 7-8, pp. 647–656, 2003.

[2] J.-H. Lee, M.-R. Lee, J.-T. Kim, V. Luk, and Y.-H. Jung, "A study of the characteristics of the acoustic emission signals for condition monitoring of check valves in nuclear power plants," *Nuclear Engineering and Design*, vol. 236, no. 13, pp. 1411–1421, 2006.

[3] E. Zio and I. C. Popescu, "Fault diagnosis of nuclear components by kohonen self-organizing maps," in *Proceedings of the 8th International Conference on Probabilistic Safety Assessment and Management (PSAM '06)*, New Orleans, La, USA, May 2006.

[4] E. Ayaz, "Component-wide and plant-wide monitoring by neural networks for Borssele nuclear power plant," *Energy Conversion and Management*, vol. 49, no. 12, pp. 3721–3728, 2008.

[5] J.-J. Jiang, L. Zhang, Y.-Q. Wang, Y.-Y. Peng, K. Zhang, and W. He, "Markov reliability model research of monitoring process in digital main control room of nuclear power plant," *Safety Science*, vol. 49, no. 6, pp. 843–851, 2011.

[6] H. M. Hashemian, "On-line monitoring applications in nuclear power plants," *Progress in Nuclear Energy*, vol. 53, no. 2, pp. 167–181, 2011.

[7] L. J. Bond, P. Ramuhalli, M. S. Tawfik, and N. J. Lybeck, "Prognostics and life beyond 60 years for nuclear power plants," in *Proceedings of the IEEE International Conference on Prognostics and Health Management (PHM '11)*, pp. 1–7, Montreal, Canada, June 2011.

[8] S. Liu and X. Y. Sheng, "Gearbox scheme in high temperature reactor helium gas turbine system," *World Journal of Nuclear Science and Technology*, vol. 2, no. 3, pp. 85–88, 2012.

[9] Z. Hameed, Y. S. Hong, Y. M. Cho, S. H. Ahn, and C. K. Song, "Condition monitoring and fault detection of wind turbines and related algorithms: a review," *Renewable and Sustainable Energy Reviews*, vol. 13, no. 1, pp. 1–39, 2009.

[10] S. Park, J. Lee, U. Moon, and D. Kim, "Failure analysis of a planetary gear carrier of 1200HP transmission," *Engineering Failure Analysis*, vol. 17, no. 2, pp. 521–529, 2010.

[11] H. W. Wang, B. Ma, L. Q. Niu, and C. S. Zheng, "The wear characteristics of thrust washer in conflux planetary gear train of power shift transmission," *Engineering Failure Analysis*, vol. 28, pp. 318–327, 2013.

[12] M. Khazaee, H. Ahmadi, M. Omid, A. Moosavian, and M. Khazaee, "Classifier fusion of vibration and acoustic signals for fault diagnosis and classification of planetary gears based on Dempster-Shafer evidence theory," *Proceedings of the Institution of Mechanical Engineers, Part E: Journal of Process Mechanical Engineering*, vol. 228, no. 1, pp. 21–32, 2014.

[13] R. Zimroz and A. Bartkowiak, "Two simple multivariate procedures for monitoring planetary gearboxes in non-stationary operating conditions," *Mechanical Systems and Signal Processing*, vol. 38, no. 1, pp. 237–247, 2013.

[14] A. Bartkowiak and R. Zimroz, "Dimensionality reduction via variables selection—Linear and nonlinear approaches with application to vibration-based condition monitoring of planetary gearbox," *Applied Acoustics*, vol. 77, pp. 169–177, 2014.

[15] C. Molina Vicuña, "Effects of operating conditions on the Acoustic Emissions (AE) from planetary gearboxes," *Applied Acoustics*, vol. 77, pp. 150–158, 2014.

[16] Z. P. Feng and M. Liang, "Fault diagnosis of wind turbine planetary gearbox under nonstationary conditions via adaptive optimal kernel time-frequency analysis," *Renewable Energy*, vol. 66, pp. 468–477, 2014.

[17] J. P. Torregrosa Koch and C. Molina Vicuña, "Dynamic and phenomenological vibration models for failure prediction on planet gears of planetary gearboxes," *Journal of the Brazilian Society of Mechanical Sciences and Engineering*, vol. 36, no. 3, pp. 533–545, 2014.

[18] Z. L. Liu, J. Qu, M. J. Zuo, and H.-B. Xu, "Fault level diagnosis for planetary gearboxes using hybrid kernel feature selection and kernel Fisher discriminant analysis," *International Journal of Advanced Manufacturing Technology*, vol. 67, no. 5-8, pp. 1217–1230, 2013.

[19] L. Hong, J. S. Dhupia, and S. W. Sheng, "An explanation of frequency features enabling detection of faults in equally spaced planetary gearbox," *Mechanism and Machine Theory*, vol. 73, pp. 169–183, 2014.

[20] J. L. Chen, C. L. Zhang, X. Y. Zhang, Y. Y. Zi, S. L. He, and Z. Yang, "Planetary gearbox condition monitoring of ship-based satellite communication antennas using ensemble multiwavelet analysis method," *Mechanical Systems and Signal Processing*, vol. 54-55, pp. 277–292, 2015.

[21] Z. P. Feng, M. Liang, Y. Zhang, and S. M. Hou, "Fault diagnosis for wind turbine planetary gearboxes via demodulation analysis based on ensemble empirical mode decomposition and energy separation," *Renewable Energy*, vol. 47, pp. 112–126, 2012.

[22] Z. P. Feng, M. J. Zuo, J. Qu, T. Tian, and Z. L. Liu, "Joint amplitude and frequency demodulation analysis based on local

mean decomposition for fault diagnosis of planetary gearboxes," *Mechanical Systems and Signal Processing*, vol. 40, no. 1, pp. 56–75, 2013.

[23] N. G. Nikolaou and I. A. Antoniadis, "Application of morphological operators as envelope extractors for impulsive-type periodic signals," *Mechanical Systems and Signal Processing*, vol. 17, no. 6, pp. 1147–1162, 2003.

[24] B. Li, P.-L. Zhang, Z.-J. Wang, S.-S. Mi, and D.-S. Liu, "A weighted multi-scale morphological gradient filter for rolling element bearing fault detection," *ISA Transactions*, vol. 50, no. 4, pp. 599–608, 2011.

[25] C. Q. Shen, Q. B. He, F. R. Kong, and P. W. Tse, "A fast and adaptive varying-scale morphological analysis method for rolling element bearing fault diagnosis," *Proceedings of the Institution of Mechanical Engineers, Part C: Journal of Mechanical Engineering Science*, vol. 227, no. 6, pp. 1362–1370, 2013.

[26] S. J. Dong, B. P. Tang, and Y. Zhang, "A repeated single-channel mechanical signal blind separation method based on morphological filtering and singular value decomposition," *Measurement*, vol. 45, no. 8, pp. 2052–2063, 2012.

[27] H. Li and D.-Y. Xiao, "Fault diagnosis using pattern classification based on one-dimensional adaptive rank-order morphological filter," *Journal of Process Control*, vol. 22, no. 2, pp. 436–449, 2012.

[28] J. Wang, Q. Zhang, and G. Xu, "Extraction of operation characteristics in mechanical systems using genetic morphological filter," *Journal of Vibroengineering*, vol. 15, no. 1, pp. 185–195, 2013.

[29] W. Tan, X. A. Chen, and S. J. Dong, "A new method for machinery fault diagnoses based on an optimal multiscale morphological filter," *Journal of Mechanical Engineering*, vol. 59, no. 12, pp. 719–724, 2013.

[30] A. S. Raj and N. Murali, "Early classification of bearing faults using morphological operators and fuzzy inference," *IEEE Transactions on Industrial Electronics*, vol. 60, no. 2, pp. 567–574, 2013.

[31] Z. W. Chen, N. Gao, W. Sun et al., "A signal based triangular structuring element for mathematical morphological analysis and its application in rolling element bearing fault diagnosis," *Shock and Vibration*, vol. 2014, Article ID 590875, 16 pages, 2014.

[32] G. Yu, C. N. Li, and J. F. Zhang, "A new statistical modeling and detection method for rolling element bearing faults based on alpha-stable distribution," *Mechanical Systems and Signal Processing*, vol. 41, no. 1-2, pp. 155–175, 2013.

[33] Stable Distribution Definition, http://en.wikipedia.org/wiki/Stable_distribution.

[34] J. P. Nolan, "An introduction to stable distributions," 2014, http://academic2.american.edu/~jpnolan/stable/stable.html.

[35] Bearing Data Sets, http://csegroups.case.edu/bearingdatacenter/pages/download-data-file.

[36] D. Wang, P. W. Tse, and K. L. Tsui, "An enhanced Kurtogram method for fault diagnosis of rolling element bearings," *Mechanical Systems and Signal Processing*, vol. 35, no. 1-2, pp. 176–199, 2013.

[37] Z. P. Feng and M. J. Zuo, "Vibration signal models for fault diagnosis of planetary gearboxes," *Journal of Sound and Vibration*, vol. 331, no. 22, pp. 4919–4939, 2012.